Process Safety and Environmental Protection 167 (2022) 21–33

Contents lists available at ScienceDirect

Process Safety and Environmental Protection

journal homepage: www.journals.elsevier.com/process-safety-and-environmental-protection

Performance evaluation and multi-criteria decision analysis of thermal energy storage integrated geothermal district heating system

Oguz Arslan [a,*], Asli Ergenekon Arslan [b]

[a] Mechanical Engineering Department, Engineering Faculty, Bilecik Seyh Edebali University, Bilecik, Turkey
[b] Quality Control in Manufacturing Programme, Mechanics and Metal Technologies Department, Vocational School, Bilecik Seyh Edebali University, Bilecik, Turkey

ARTICLE INFO

Keywords:
Efficiency analysis
Exergy analysis
District heating
Geothermal
Thermal energy storage

ABSTRACT

Geothermal energy use in district heating systems has been prevalent and familiar in areas with rich sources for many years. In conventional geothermal district heating systems (GDHS), the geothermal fluid is transported to a heat center to give its heat energy to the secondary fluid. Then, this secondary fluid is circulated in the city network to give its heat energy to the heating circuit by the heat exchangers in the substations. Finally, the geothermal fluid is re-injected to handle the continuity of the resources. This current system works under the designed conditions of a heating system with significant electricity consumption and enormous heat waste. In this study, a thermal energy storage (TES) system was integrated into substations instead of heat exchangers to prevent the waste of heat and overconsumption of electricity by obtaining just-in-time working conditions. In this regard, a shell and tube latent heat TES system was designed for residential use for peak loads and integrated into the heating circuit of GDHS, preserving the current main structure. A number of 37 available cases were formed parametrically to evaluate the system's performance. These cases were analyzed thermodynamically by energy and exergy methods. The net present value (NPV) method was used to evaluate the cases' economics. Finally, an efficiency analysis technique with output satisficing (EATWOS) was conducted to determine the most efficient design from the viewpoints of exergy efficiency, NPV, and CO_2 emissions.

1. Introduction

Thermal energy storage (TES) has been a popular research area in recent years. It is a valuable tool since a TES unit enables to use of required energy stored from the waste heat and renewable energy sources. So, it is preferred in many systems, from electric vehicles to buildings.

Studies about TES in district heating systems (DHS) increased over the last years. Knudsen et al. (2021). investigated the TES use in DHS. They proposed a predictive control approach for sizing TES sourced by industrial waste heat. They determined that it is possible to achieve a 12% reduction of effective peak-heating with a TES volume of 1500 m^3. Dahash et al. (2021). investigated a large-scale TES system integrated into DHS powered by renewable energy from a techno-economical point of view. They concluded that high-temperature DHS with a large-scale TES system was less economical than the low-temperature one depending on the insulation costs. Mäki et al. (2021). investigated a small-scale TES-based DHS powered by solar energy. The stored energy was later fed to the heating network fluid, aided by biomass and fuel oil energy for the peak loads. They indicated that the TES sourced by solar energy (with a share of 15–25%) in the DHS increased the costs and emissions. Siddiqui et al. (2021). investigated the impact of large-scale heat pumps in DHS. They also integrated a TES system into DHS to provide flexibility of operation. They concluded that a TES capacity of 1% reduces the electricity peak loads. Cunha et al. (2022). investigated the integration of portable TES systems into DHS. The TES system was fed by industrial waste heat. They also compared the proposed system with a conventional pipeline system. As a result, they concluded that the pipeline system is more economical than the TES-integrated one. They indicated that this was due to the higher costs of the daily replacement of TES. Rezaie et al. (2015). investigated the role of TES in DHS. They conducted a case study for the Friedrichshafen district energy system using the exergy method. The handled TES system was fed by solar energy. As a result, they concluded an energy and exergy efficiency of 60% and 19%, respectively. He et al. (2022). optimized the space heating system with TES. The TES system was fed by solar and electrical energy. According to the optimum solution, CO_2 emissions can be reduced by 5480.6 $kgCO_2eq$ per year with a payback period of 3.7 years. Saloux and Candanedo (Saloux and Candanedo, 2021) investigated

* Corresponding author.
E-mail addresses: oguz.arslan@bilecik.edu.tr (O. Arslan), asli.arslan@bilecik.edu.tr (A.E. Arslan).

https://doi.org/10.1016/j.psep.2022.08.073
Received 31 July 2022; Received in revised form 28 August 2022; Accepted 31 August 2022
Available online 5 September 2022

Nomenclature

A	area (m^2).
B	cash flow ($).
C	cost ($).
E	Multi-criteria efficiency.
$\dot{E}$	energy rate (kW).
$\dot{E}x$	exergy rate (kW).
Gr	Grashof number.
h	Convective heat transfer coefficient (W/m^2K) or specific enthalpy (kJ/kg).
ip	distance matrices for input.
I	investment cost ($).
k	conductive heat transfer coefficient (W/mK).
$\dot{m}$	mass flow rate (kg/s).
n	number of plate or pipe.
Nu	Nusselt number.
op	distance matrices for output.
P	pressure (kPa, bar, or atm).
Pr	Prandtl number.
$\dot{q}$	heat rate per length (kW/m).
$\dot{Q}$	heat rate (kW).
r	radius (m) or normalized output.
Ra	Rayleigh number.
Re	Reynolds number.
s	specific entropy (kW/kgK) or normalized input.
T	temperature (K or °C).
U	Total heat transfer coefficient (W/m^2K).
v	weight for output.
w	weight for input.
$\dot{W}$	work rate (kW).
x	input value.
$\underline{X}$	input matrices.
y	output value.
$\underline{Y}$	output matrices.

Greek symbols

β	Volumetric expansion coefficient (-).
ε	exergy efficiency (%).
η	energy efficiency (%).
μ	dynamic viscosity (Ns/m^2).
ν	Specific volume (m^3/kg).
ρ	density (kg/m^3).
ψ	specific flow exergy (kJ/kg).

Subscripts

d	destruction.
D	diameter.
i	inlet or i^{th} component.
ins	insulation.
k	k^{th} component.
lm	logarithmic mean.
o	outlet.
T	value at a specified temperature.
0	value at the reference state.

Superscripts

Q	exergy term related to heat.
W	exergy term related to work.
o	standard.

Abbreviations

C	Heat center.
DHS	District heating system.
GDHS	Geothermal district heating system.
HC	Heating circuit.
H-line	Heating zone transmission line.
NPV	Net present value.
PCM	Phase change material.
S	Substation.
T-line	Geothermal zone transmission line.
TES	Thermal energy storage.

minimizing the primary energy use in solar DHS with seasonal TES. They determined an annual saving of 47% on pump electricity use by the proposed model-based predictive control strategy. The reduction of energy costs and greenhouse gases were reported as 38% and 32%, respectively. Dorotić et al. (2019). optimized the DHS with short-term and seasonal TES in economic, environmental, and exergetic factors. The TES was fed by several energy sources such as waste heat of natural gas boilers, cogeneration, electrical energy, waste heat of biomass boilers and solar energy. An exergy efficiency up to 65% was reported when high solar thermal production was an issue. Li et al. (2021). investigated TES integration into the DHS. The waste heat of data centers fed the TES. They considered water tank and borehole for short-term and long-term storage, respectively. According to the results, the water tank case shaved 31% of the peak load with an annual saving of 5% and a payback period of fewer than 15 years. No obvious benefit in CO_2 reduction was recorded in this case. For the borehole storage case, a waste heat utilization of up to 96% was achieved with a CO_2 reduction of 8%. All these studies show that TES integration into DHS would positively affect the system from the environmental, economic, and energy efficiency points of view.

Literature about TES integration shows that the planning is based on seasonal energy storage. In this regard, periodic renewable sources such as solar energy are the practical solutions; the energy can be stored when available and used in the heating season. On the other hand, the planning of TES systems is based on short-term applications to aid the peak load requirements. The waste heat of combustion products or electricity is commonly considered in these schedules. Also, it is possible to use TES systems in DHS powered by non-periodic (continuous) sources, such as geothermal energy. In literature, there are limited studies on this issue. Matuszewska et al. (2020). investigated the technical and economical possibility of geothermal heating including a mobile TES system (M-TES) in the southern part of Poland. They indicated that distance is a significant factor in economic profitability. They also indicated that M-TES is quite effective in the reduction of CO_2 emissions and profitable in distances around 3–4 km. Halaj et al. (2022). studied an aquifer thermal energy storage (ATES) system to increase the energy efficiency of geothermal energy systems in terms of different temperature differential scenarios. The study indicates that the ATES is profitable for efficient use of the energy source where the geothermal potential for direct purposes is low. Kim et al. (2018). investigated the integration of the TES system with a geothermal heat pump system. In the study, the case with TES was compared with the case without TES. They indicate that it is viable to reduce the operational cost by 36–54%. Huang et al. (2021). investigated high-temperature aquifer thermal energy storage (HT-ATES) for the reduction of greenhouse gases. They showed that the ATES system is an economic and efficient tool to reduce emissions since it buffers seasonal imbalances. Hemmatabady et al. (2022). investigated the integration of a borehole TES system into DHS from environmental and economic points of view. As a passive heating system, the heat obtained from solar energy is stored in the borehole heat exchangers to heat 52 single residences in the winter season. As an active heating system, the stored geothermal energy was boosted by heat pumps. Gas

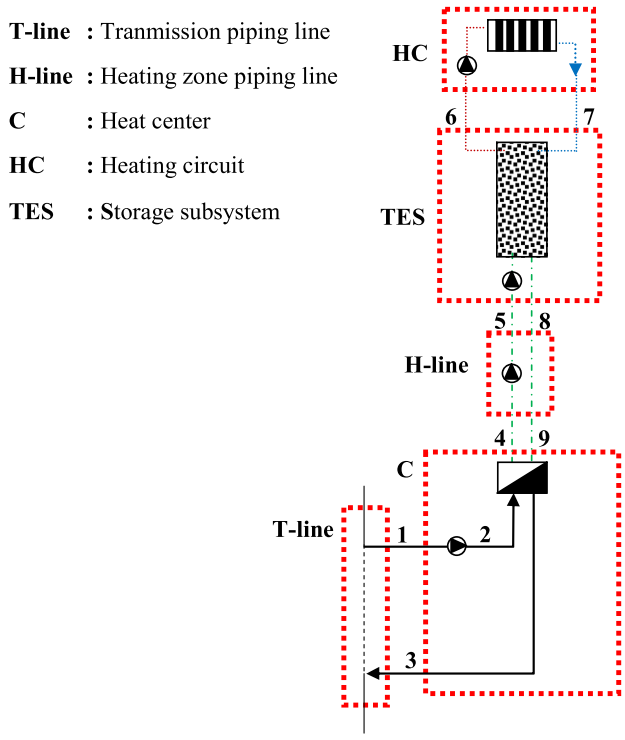

Fig. 1. Flow diagram of TES-based S-GDHS.

boilers also aid the system for peak loads. Kyriakis and Younger (Kyriakis and Younger, 2016) investigated TES integration into geothermal district heating systems (GDHS) to increase geothermal energy utilization. The control strategy was handled to cover a part of the peak loads to decrease the usage of peak-up boilers. According to the study, two TES systems, namely hot and cold storage, were integrated into the main transmission lines of the secondary circuit (the circuit after the heat center). As a result, it was found that the proposed system is beneficial since it decreased heating costs and emissions. These studies show that TES is a valuable tool to boost the energy level of the other sources or meet the peak loads for extreme climatic conditions.

These scenarios are not effective solutions for the DHS powered by geothermal fluid energy since the fluid is circulated in continuous and stable conditions. Such systems are commonly used in areas with large geothermal reservoirs, as in the Simav geothermal region in Turkey. These systems are designed for peak loads according to the meteorological conditions of the districts. These systems have a simple structure in which the heat energy is transferred from wells to buildings and work under constantly designed conditions. This situation means that the system operates continuously, although there is no need for peak requirements. Under these working conditions, two expected problems are the overconsumption of electricity and large waste heat (Cabeza and Palomba, 2022; Arslan et al., 2009a). In this regard, thermal energy storage (TES) systems can be an alternative solution. In this study, a new geothermal district heating system was designed by integrating a residential-scale latent heat TES system into the Simav GDHS (S-GDHS). For this purpose, a new shell and tube type TES system was designed for the residences on a small scale. This new design includes simultaneous charging and discharging by the heating and cooling pipes. A total of 37 different designs were formed and analyzed employing energy and exergy methods. The designs were then investigated from an economic point of view by the net present value (NPV) method. An environmental evaluation was also conducted for the designs. Finally, the best design was determined by the multi-criteria decision-making analysis method of EATWOS in terms of NPV, exergy efficiency, and CO_2 reduction as the objective functions.

2. Material and method

The integrated usage of the Simav geothermal resources, located in the Simav graben system in Turkey, was considered for the TES-based SGDHS. Simav geothermal wells provide a source with a mass flow rate of 462.0 kg/s and a temperature of 133.5 °C (Arslan and Kose, 2010). The S-GDHS was planned to generate heat for 12,500 residences. The flow diagram of the TES-based S-GDHS is given in Fig. 1.

According to the designed system, geothermal water is used to heat residences after the electricity generation process. S-GDHS includes five parts, namely the geothermal transmission line (T-line), heat center (C), heating zone transmission line (H-line), TES substation (TES), and heating circuit (HC). The geothermal water is transported to C via pre-insulated pipes with a 4250 m length (point 1). After transferring its heat to the circulating water of the heating zone (point 3), the fed fluid is given to the T-line for another loop in the integrated system (point 3). The heated circulating water (points 4–5) is transferred to TES substations of the buildings via pre-insulated pipes with a 4000 m length (the farthest residence). The water is then transferred to C (points 8–9) to complete the heating cycle. The heated circuit water (points 5–8) transfers its heat to a latent heat TES system. The stored heat is then used for the heating requirements of the residences (points 6–7) via aluminum panel radiators with a height of 600 mm. Under these circumstances, the S-GDHS system was evaluated from the energy, exergy, economic and environmental points of view. The calculation steps are given in Fig. 2.

2.1. Heating requirements of residences

In terms of the heat transfer coefficient (U_i) and heat transfer area (A_i) of the building structures (namely wall, window, ceiling, and floor), and temperature difference (ΔT) between indoor and outdoor, the heat requirement of a residence is determined as follows:

$$\dot{Q}_{demand} = \sum_i (U \bullet A \bullet \Delta T)_i \quad (1)$$

Here the U values were determined considering the allowed limits of the related standards (TSE (TSE (Turkish Standards Institution)), 2008). According to this, U values of the wall, window, ceiling, and floor were assumed to be 0.5 W/m^{2}K, 2.4 W/m^{2}K, 0.3 W/m^{2}K, and 0.45 W/m^{2}K, respectively. The residence equivalence was assumed to be 100 m^2 with a 96 m^2 wall area and 24 m^2 window area. According to related standards, the outdoor design temperature was taken as − 12 °C, whereas it was taken as 10 °C for the unheated spaces next to ceilings and floors. According to these assumptions, the designing heat demand of the residences ($\dot{Q}_{design}$) was calculated to be 56,130 kW, which means approximately 4.5 kW for each residence. It was also assumed that the heating process starts when the daily average outdoor temperature is less than 15 °C (TSE (TSE (Turkish Standards Institution)), 2008). The daily average temperatures were calculated using the Simav region's five-year values. The daily average outdoor air temperatures, soil temperature (at 0.5 m depth) and daily heat demands are given in Fig. 3 (MSTS Meteorological Service of Turkish State, 2022a, 2022b).

According to Fig. 3, the heat demand of the residences ($\dot{Q}_{demand}$) ranges between 20,675 kW and 44,936 kW during the heating season, with the daily average outdoor temperature ($T_{outdoor}$) ranging between − 3.5 °C and 14.9 °C. Therefore, the number of heating days was determined to be 209 days per year. The soil (T_{soil}) temperature is also an important parameter since it directly affects the heat losses of transmission pipes placed underground. The average soil temperature ranges between 5.8 °C and 20.2 °C.

2.2. TES system design

The TES system was taken of the latent heat storage type. It was

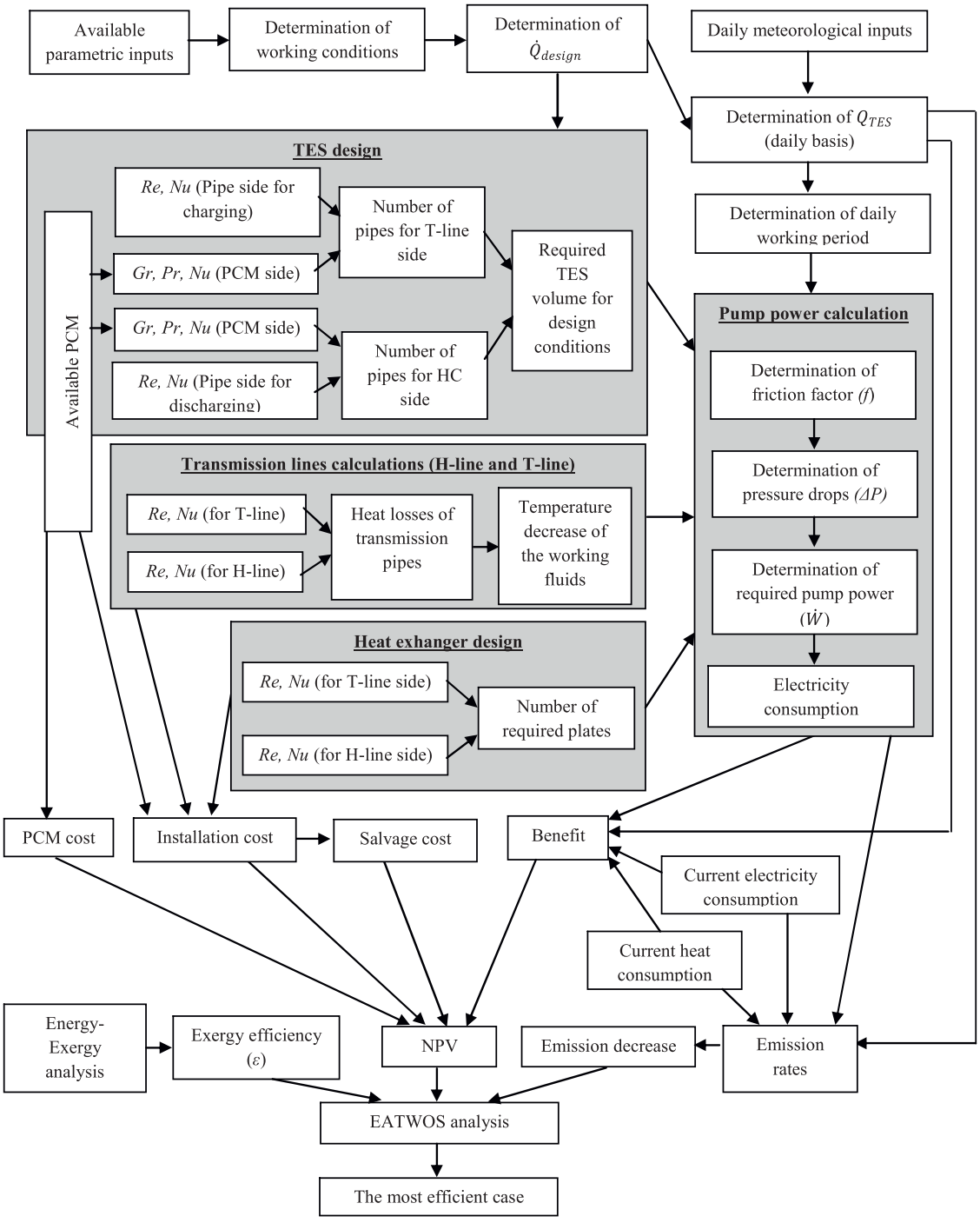

Fig. 2. Calculation flow chart.

designed considering a shell and pipe structure. The structure of the TES system is given in Fig. 4.

According to Fig. 4, the TES system is composed of heating pipes (1), Phase Change Material (PCM) (2), cooling pipes (3), shell structure (4), insulation material (5), and outer cover (6). The properties of the TES structure are given in Table 1.

The selected phase change material was paraffin since it is commonly used in buildings depending on economic and environmental factors. Also, paraffin is friendlier for the structural materials of the TES system and has higher heat storage capacities (RUBITHERM, 2022). The kind of paraffin was determined considering the operational parameters of the DHS. The properties of the used PCMs are given in Table 2 (RUBITHERM, 2022; Tenpierik et al., 2019).

The volume of the TES system was calculated by taking the required PCM amount into account. Also, the heating (n_1) and cooling pipes (n_2) volume was considered in the system volume. The total volume of the TES system is the sum of the pipes volume (V_{pipe}) and PCM volume (V_{PCM}):

$$V_{TES} = \overbrace{\left(A_{pipe} \bullet (n_1 + n_2) \bullet H\right)}^{V_{pipe}} + \overbrace{\left(\frac{86400 \bullet \dot{Q}_{design}}{Q_{TES}} \bullet \beta\right)}^{V_{PCM}} \quad (2)$$

where A_{pipe} is the cross-sectional area of the heating and cooling pipes. H is the height of the TES system and was taken as 1.5 m considering the conditions of residential substations. β is the volumetric expansion rate

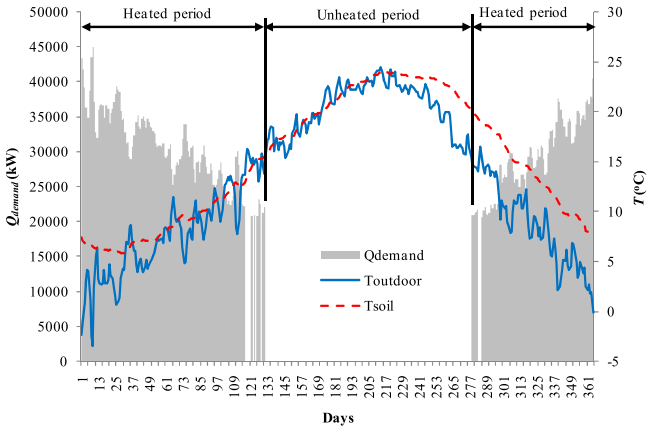

Fig. 3. Variation of outdoor temperature, soil temperature and heat demand of residences (MSTS Meteorological Service of Turkish State, 2022a, 2022b).

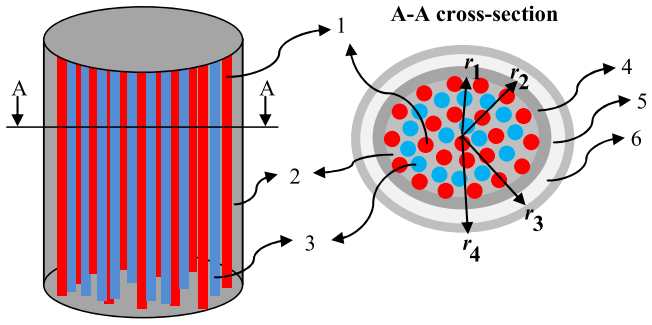

Fig. 4. Structure of TES system.

of PCM during the phase change, which depends on the specific volumes of solid and liquid phases given in Table 2. Q_{TES} indicates the daily heat transfer rate (see Table 2) for a PCM and is given as follows:

$$Q_{TES} = Q_{latent} + Q_{sensible} \tag{3}$$

Here, Q_{latent} is taken from Table 2 (RUBITHERM, 2022). $Q_{sensible}$ depends on the operating temperature range determined parametrically and is given as follows in terms of specific heat:

$$Q_{sensible} = C_p\left(\Delta T_{upper} + \Delta T_{lower}\right) \tag{4}$$

where ΔT_{upper} and ΔT_{lower} indicate the upper working conditions. Taking the melting point into account, these temperature differences are calculated as follows:

$$\Delta T_{upper} = T_{upper} - T_{melting} \tag{5}$$

$$\Delta T_{lower} = T_{melting} - T_{lower} \tag{6}$$

In Eqs. 5 and 6, the minimum value of T is determined according to the DHS parameters. The maximum value of T is also determined in the same way; however, the maximum working temperature of the PCM is considered when it exceeds this point (see Table 2). The numbers of heating and cooling pipes are calculated in terms of the pipes' required heat transfer area (lateral area). The required area is calculated as follows:

$$A_{pipe} = \frac{\dot{Q}_{design}}{12500 \bullet U_{pipe} \bullet \left[\left(\frac{T_5+T_8}{2}\right) - \left(\frac{T_6+T_7}{2} + 5\right)\right]} \tag{7}$$

In Eq. 7, temperature differences were taken as the average of inputs and outputs values of the HC and H-line. Additionally, a temperature difference of 5 °C was added for an effective heat transfer between the working fluids and PCM. The heat transfer coefficient between the working fluid and PCM (U_{pipe}) is given by:

$$U_{pipe} = \frac{1}{\frac{1}{h_i} + \frac{r_i}{k_{pipe}} ln\left(\frac{r_o}{r_i}\right) + \frac{r_o}{r_i}\frac{1}{h_o}} \tag{8}$$

Here, k_{pipe}, r_i, and r_o indicate the pipes' heat conduction coefficient, inner diameter, and outer diameter, respectively. h_i and h_d are respectively the convective heat transfer coefficients of the working fluid and PCM and are calculated in terms of Nusselt (Nu) number given by (Yuncu and Kakac, 1999):

$$h = \frac{Nu \bullet k}{D} \tag{9}$$

where h, k, and D indicate the convective heat transfer coefficient of the related fluid, conductive heat transfer coefficient of the pipe, and diameter, respectively. The Nu number of the working fluid side for laminar flow and constant wall temperature is given by (Yuncu and Kakac, 1999):

Table 1
Properties of TES system.

ComponentComponent	Explanation	Material	Diameter (mm)	Thickness (mm)	k (W/mK)
1	Heating pipe	St37	25	4	170
2	–	PCM	–	–	–
3	Cooling pipe	St37	25	4	170
4	Shell	St37	*	3	170
5	Insulation	Rock wool	–	100	0.035
6	Cover	Al (Embossed)	*	1	237

* Variates with the design parameters.

Table 2
Properties of used PCMs (RUBITHERM, 2022; Tenpierik et al., 2019).

PCM	ρ_{solid} (m^3/kg)	ρ_{liquid} (m^3/kg)	β	$T_{melting}$ (°C)	Q_{Latent} (kJ/kg)*	C_p (kJ/kgK)	T_{lower} (°C)	T_{upper} (°C)	T_{max} (°C)	k (W/mK)	μ (kg/ms)
RT42	880	760	1.16	42	130	2	47	72	72	0.2	0.01
RT44HC	800	700	1.14	43	220	2	48	70	70		
RT47	880	770	1.14	47	130	2	52	65	65		
RT50	880	760	1.16	50	130	2	55	70	70		
RT54HC	850	800	1.06	54	170	2	59	85	85		
RT55	880	770	1.14	55	140	2	60	90	90		

*Calculated according to the given working temperature range of Ref (RUBITHERM, 2022).

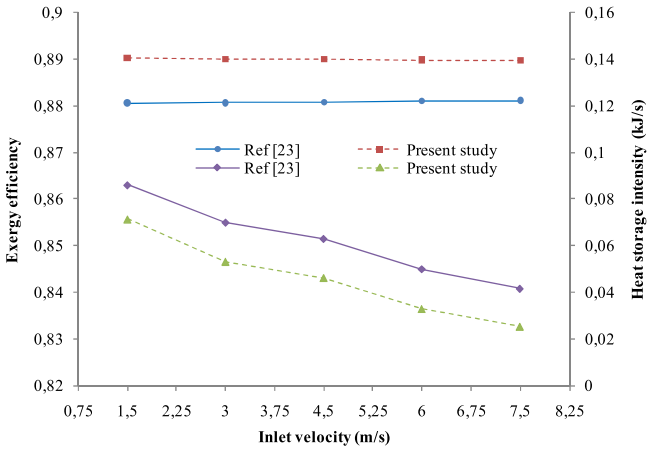

Fig. 5. Model validation.

$$Nu = 3.66 \tag{10}$$

Under natural convection conditions, the *Nu* number for the PCM side is given by (Bertrand et al., 1999):

$$Nu = 0.33 \bullet (Gr \bullet Pr)^{0.25} \quad for \quad Pr \gg 1 \quad and \quad 10^8 < Gr < 10^8 \tag{11}$$

where *Gr* and *Pr* are the Grashof and Prandtl number, respectively and given by:

$$Gr = \frac{g\beta\Delta TH^3}{\left(\frac{\mu}{\rho}\right)^2} \tag{12}$$

$$Pr = \frac{\mu C_p}{k} \tag{13}$$

where g and μ indicate the gravitational acceleration and dynamic viscosity, respectively. Finally, the number of pipes can be calculated as:

$$n_{pipe} = \frac{A_{pipe}}{\pi DH}$$

The mentioned calculation procedure is separately applied for both heating and cooling pipes since the working fluids of the heating mode come from the H-line, whereas that of the cooling mode comes from the HC. The heat loss from the TES system is added to the sink fluid of the H-line. It is calculated as follows:

$$\dot{Q}_{TES,loss} = U_{TES}A_{TES}\left(T_{TES} - T_{ambinece}\right) \tag{14}$$

where U_{TES} and A_{TES} are the heat transfer coefficient and lateral area of the TES shell, respectively. T_{TES} is handled as the average temperature of the PCM's upper and lower working temperature according to parametric conditions. $T_{ambiance}$ is, considering the worst case conditions, taken as 0 °C for the substation as the non-heated space. According to Fig. 3, the heat transfer coefficient of the TES shell is calculated by:

$$U_{TES} = \frac{1}{\frac{1}{h_i} + \frac{r_1}{k_4} ln\left(\frac{r_2}{r_1}\right) + \frac{r_1}{k_5} ln\left(\frac{r_3}{r_2}\right) + \frac{r_1}{k_6} ln\left(\frac{r_4}{r_3}\right) + \frac{r_4}{r_1}\frac{1}{h_o}} \tag{15}$$

where h_i are the convective heat transfer coefficients of the PCMs. h_o is the convective heat transfer coefficient of the environment of the substation space, and the heat resistance value related to this value ($1/h_o$) is taken as 0.17 m^2K/W (TSE (TSE (Turkish Standards Institution)), 2008). The conductive heat transfer coefficients of the shell (k_4), insulation (k_5), and cover (k_6) are mentioned in Table 2. The installed model was validated using the data from Wu et al. (2022). The data was obtained by the matching method, and the results are shown in Fig. 5.

According to Fig. 5, the results of the present study are in good agreement with those of Wu et al. (2022). The calculated *Nu* number (53.73) is in good agreement with the data of Mohaghegh et al. (2022).

2.3. Heat exchanger design

In the heat center, a plate-type heat exchanger (HE-C) was used to transfer the energy of the geothermal fluid to the H-line fluid. The plate-type heat exchanger (HE-sub) was also considered in the substations to compare the old and new designs. In the designing procedure, the required plate numbers are determined. In this regard, the designs help to calculate the pressure drops and required pump power. The calculation procedure of the heat exchanger is given as follows:

$$n_{plate} = \frac{A_{HE-C}}{A_{plate}} \tag{16}$$

where $A_{HE\text{-}C}$ and A_{plate} indicate the required total heat transfer area and area of a single plate, respectively. A_{plate} was included in calculations as 1.38 m^2 (Jiangyin, 2022a). Assuming an efficiency of 98%, $A_{HE\text{-}C}$ is calculated by:

$$A_{HE-C} = \frac{\dot{Q}_{geothermal}0.98}{U_{HE-C}\Delta T_{lm}} = \frac{0.98\dot{m}_2(h_2 - h_3)}{U_{HE-C}\Delta T_{lm}} \tag{17}$$

where h, $U_{HE\text{-}C}$ and ΔT_{lm} are the enthalpy, the heat transfer coefficient of the heat exchanger and logarithmic mean temperature difference, respectively. $U_{HE\text{-}C}$ and ΔT_{lm} are given by:

$$U_{HE-C} = \frac{1}{\frac{1}{h_i} + R_i + \frac{l}{k_{plate}} + R_o + \frac{1}{h_o}} \tag{18}$$

$$\Delta T_{lm} = \frac{(T_2 - T_4) - (T_3 - T_9)}{ln\left(\frac{T_2 - T_4}{T_3 - T_9}\right)} \tag{19}$$

In Eq. 18, k_{plate} is the conductive heat transfer coefficient of the aluminum plate and was taken as 54 W/mK (Genceli, 1999). The fouling resistance of both cold (R_i) and hot (R_o) streams is assumed as 0.0002 m^2K/W (Genceli, 1999). The convective heat transfer coefficients of the hot (h_o) and cold (h_i) streams are calculated in terms of *Nu* number as given in Eq. 9. (h_o) and cold (h_i) are calculated as follows (Yuncu and Kakac, 1999):

$$Nu = 0.2 \bullet Re^{0.67} \bullet Pr^{0.4} \bullet \left(\frac{\mu}{\mu_o}\right)^{0.1} \tag{20}$$

where μ_o indicates the dynamic viscosity at the average temperature of both the hot and cold streams. For the substation heat exchangers, the same calculation procedure is followed. However, A_{plate} was included in calculations as 0.26 m^2 at this stage (Jiangyin, 2022b). In the calculation of the *Re* number, the hydraulic diameter (D_h) is used instead of diameter (D), which was taken as 0.0139 m for the C side and 0.0137 m for the substation side (Jiangyin, 2022a, 2022b).

2.4. Heat losses of transmission lines

The calculation procedure of the heat losses per unit length in the pipelines can be given as follows:

$$\dot{q}_{loss} = \frac{2\pi(T_i - T_o)}{\frac{1}{r_1 h_i} + \frac{1}{k_{pipe}} ln\left(\frac{r_2}{r_1}\right) + \frac{1}{k_{ins}} ln\left(\frac{r_3}{r_2}\right) + \frac{1}{k_{cover}} ln\left(\frac{r_4}{r_3}\right) + \frac{1}{k_{soil}} ln\left(\frac{r_5}{r_4}\right)} \tag{21}$$

where T_i and T_o indicate the fluid and soil temperatures. The soil temperature was taken as 5.5 °C in the calculations according to Fig. 4. k_{pipe}, k_{ins}, k_{cover}, and k_{soil} are conduction coefficients of the pipe material (St-37 steel), an insulation layer (polyurethane), covering material (polyethylene), and soil layer respectively. These values are taken as 76 W/mK, 0.028 W/mK, 0.43 W/mK and 2.1 W/mK, respectively (Arslan

et al., 2009a; Arslan and Kose, 2010). The term r indicates the radius of the pipe layers. In the H-line, these values are 0.15 m, 0.1556 m, 0.23 m, and 0.2352 m for r_1, r_2, r_3, and r_4, respectively. The value of r_5 is taken as 0.6 m, where the soil temperature is not affected by the heat losses of the pipes (Arslan and Kose, 2010). h_i is the convective heat transfer coefficient of the fluid and is calculated by:

$$\alpha_i = \frac{Nu \bullet k_{fluid}}{2r_i} \tag{22}$$

where is Nusselt number and given by (Yuncu and Kakac, 1999):

$$Nu = 0.012\left(Re_D^{0.8} - 280\right)Pr^{0.4} \tag{23}$$

where Pr is Prandtl number (Yuncu and Kakac, 1999). Re_D is Reynolds number and given in terms of mass flow rate:

$$Re_D = \frac{4\dot{m}}{\mu\pi D} \tag{24}$$

In the T-line, a similar procedure is followed. The values of r_1, r_2, r_3, and r_4 are 0.20 m, 0.2063 m, 0.28 m, and 0.2806 m. The temperature decrease depending on heat loss at the non-operational conditions is given by:

$$\Delta T = \frac{\dot{q}_{loss} \bullet A \bullet 86400}{mC_p} \tag{25}$$

where A is the lateral area of the transmission lines, m is the mass of the fluid in the total volume, and C_p is the specific heat of the water. The total volume was calculated based on the farthest point of the system (4000 m). Besides, a temperature decrease on the basis of daily full-time non-operational conditions is considered to handle the worst case scenario. The T-line was not included in the calculations since it also feeds the other systems such as power cycle, greenhouse heating, and spas.

2.5. Pressure drops

Pressure drops should also be taken into account since it determines the required power of the pumps. The common pressure drop is given by:

$$\Delta P = f\frac{L}{D}\frac{\rho V^2}{2} \tag{26}$$

where L and D (or Dh) indicate the length of the pipes (or plates). f denotes the friction factor and is given in terms of Reynolds number (Re) for the TES system as (Genceli, 1999):

$$f = \frac{64}{Re} \quad for \quad Re < 2300 \tag{27}$$

The friction factor is separately considered for both the heating and cooling pipes of the TES system since the feeding pumps belong to different cycles, namely the H-line and HC. In the heat exchangers, the friction factor is given by (Genceli, 1999):

$$f = \frac{1.22}{Re^{0.252}} \tag{28}$$

The pressure drops in the pipes of the T-line and H-line were also taken into account since it is variable depending on the changing parameters. The friction factor is obtained from Moody's diagram (Cengel and Boles, 2018). Finally, the required pump power is given as:

$$\dot{W} = \frac{\dot{m}v\Delta P}{\eta} \tag{29}$$

where η is the pump efficiency and is assumed as 80%.

Table 3
Energy balance equations for TES-based S-GDHS.

Components	Energy balance	Efficiency
T-line	$\dot{Q}_{T-line} = \dot{m}h_2 - \dot{m}h_1 - \dot{W}_{pump}$	$\eta = \frac{(\dot{m}h_2)}{\dot{m}h_1 + \dot{W}_{pump}}$
C	$\dot{Q}_C = (\dot{m}h_9 - \dot{m}h_4) - (\dot{m}h_3 - \dot{m}h_2) - \dot{W}_{pump}$	$\eta = \frac{(\dot{m}h_9 - \dot{m}h_4)}{(\dot{m}h_3 - \dot{m}h_3) + \dot{W}_{pump}}$
H-line	$\dot{Q}_{H-line} = (\dot{m}h_5 + \dot{m}h_9) - (\dot{m}h_4 + \dot{m}h_8) - \dot{W}_{pump}$	$\eta = \frac{(\dot{m}h_5 + \dot{m}h_9)}{(\dot{m}h_4 + \dot{m}h_8) + \dot{W}_{pump}}$
TES	$\dot{Q}_{TES} = (\dot{m}h_6 - \dot{m}h_7) - (\dot{m}h_5 - \dot{m}h_8) - \dot{W}_{pump}$	$\eta = \frac{(\dot{m}h_6 - \dot{m}h_7)}{(\dot{m}h_5 - \dot{m}h_8) + \dot{W}_{pump}}$
HC	$\dot{Q}_{useful} = \dot{m}h_7 - \dot{m}h_6$	$\eta = \frac{\dot{Q}_{useful}}{(\dot{m}h_6 - \dot{m}h_7) + \dot{W}_{pump}}$
Overall system		$\eta = \frac{\dot{Q}_{useful}}{(\dot{m}h_1 - \dot{m}h_3) + \dot{W}_{pump,total}}$

Table 4
Exergy balance equations for TES-based S-GDHS.

Components	Exergy balance	Efficiency
T-line	$\dot{E}x_{d,T-line} = (\dot{m}\psi_1 - \dot{m}\psi_2) + \dot{W}_{pump} - \left(1 - \frac{T_0}{T_{ave}}\right)\dot{Q}_{T-line}$	$\varepsilon = 1 - \frac{\dot{E}x_{d,T-line}}{\dot{m}\psi_1 + \dot{W}_{pump}}$
C	$\dot{E}x_{d,C} = (\dot{m}\psi_2 + \dot{m}\psi_9) - (\dot{m}\psi_3 + \dot{m}\psi_4) + \dot{W}_{pump} - \left(1 - \frac{T_0}{T_{ave}}\right)\dot{Q}_C$	$\varepsilon = 1 - \frac{\dot{E}x_{d,HCent}}{(\dot{m}\psi_2 + \dot{m}\psi_9) + \dot{W}_{pump}}$
H-line	$\dot{E}x_{d,H-line} = (\dot{m}\psi_4 + \dot{m}\psi_8) - (\dot{m}\psi_5 + \dot{m}\psi_9) + \dot{W}_{pump} - \left(1 - \frac{T_0}{T_{ave}}\right)\dot{Q}_{H-line}$	$\varepsilon = 1 - \frac{\dot{E}x_{d,H-line}}{(\dot{m}\psi_4 + \dot{m}\psi_8) + \dot{W}_{pump}}$
TES	$\dot{E}x_{d,TES} = (\dot{m}\psi_5 + \dot{m}\psi_7) - (\dot{m}\psi_8 + \dot{m}\psi_6) + \dot{W}_{pump} - \left(1 - \frac{T_0}{T_{ave}}\right)\dot{Q}_{TES}$	$\varepsilon = 1 - \frac{\dot{E}x_{d,TES}}{(\dot{m}\psi_5 + \dot{m}\psi_7) + \dot{W}_{pump}}$
HC	$\dot{E}x_{d,HC} = (\dot{m}\psi_6 - \dot{m}\psi_7) + \dot{W}_{pump} - \left(1 - \frac{T_0}{T_{ave}}\right)\dot{Q}_{useful}$	$\varepsilon = 1 - \frac{\dot{E}x_{d,HC}}{\dot{m}\psi_7 + \dot{W}_{pump}}$
Overall system	$\dot{E}x_{d,total} = \dot{E}x_{d,T-line} + \dot{E}x_{d,C} + \dot{E}x_{d,TES} + \dot{E}x_{d,HC}$	$\varepsilon = 1 - \frac{\dot{E}x_{ud,total}}{(\dot{m}\psi_1) + \dot{W}_{pump,total}}$

2.6. Energy and exergy analysis

The general mass and energy balances of any control volume under steady-state conditions are given by:

$$\sum \dot{m}_i - \sum \dot{m}_o = 0 \tag{30}$$

$$\dot{Q} - \dot{W} + \sum \dot{m}_i h_i - \sum \dot{m}_o h_o = 0 \tag{31}$$

where $\dot{Q}$ is the heat rate term, $\dot{W}$is the work term, $\dot{m}$ is the mass flow rate. i indicates the inlet conditions, and o indicates the outlet conditions. The energy balance equations for the considered GDHS are given in Table 3.

The exergy balance for the k^{th} component of the system is given as:

$$\dot{E}x_k^Q - \dot{E}x_k^W - \sum(\dot{m}_i\psi_i)_k - \sum(\dot{m}_o\psi_o)_k - \dot{E}x_{d,k} = 0 \tag{32}$$

where $\dot{E}x_k^Q$, $\dot{E}x_k^W$, $\dot{E}x_{d,k}$ and ψ respectively describe the exergy of heat, the exergy of the work, exergy destruction and the specific exergy of flow for the k^{th} component, and are given as:

$$\dot{E}x_k^Q = \left(1 - \frac{T_0}{T}\right)\dot{Q}_k \tag{33}$$

Table 5
Basis of the emissions (Arslan et al., 2022; Arslan and Erbas, 2021).

Source	Emission			
	CO_2	CO	NO_2	SO_2
Natural gas*	1.95023	0.00024	0.03384	–
Lignite**	0.47848	0.01418	0.00782	0.00077

* per kmole-fuel,
** per kg-fuel.

$$\dot{E}x_k^W = \dot{W}_k \tag{34}$$

$$\psi = (h - h_0) - T_0(s - s_0) \tag{35}$$

Here, h and s indicate orderly enthalpy and entropy at a particular state. Subscript 0 indicates the reference state conditions. The exergy balance equations for the TES-based S-GHDS are given in Table 4.

In Table 2, the overall exergy efficiency was calculated by taking the heat exergy of the panel radiators into account since the end product of the system is the heat energy (Arslan et al., 2009b; Ucar and Arslan, 2021).

2.7. Net present value (NPV) analysis

NPV is a valuable tool for the economic analysis of energy systems since it considers the time value of the cash flow measured in today's currency (Arat and Arslan, 2017a; Akbulut et al., 2021). *NPV* is given by:

$$NPV = \sum_{t=0}^{n} \frac{B_t}{(1+r)^t} - I \tag{36}$$

where *r, n, t, I,* and B_t are the discount rate, the lifetime of the system, related year, investment cost, and cash flow, respectively. *n* was taken as 20 years, whereas r was taken as 15.75% in the study (Arat and Arslan, 2017b; CBRT Central Bank of Republic of Turkey, 2022). B_t includes the yearly costs of operating and maintenance ($C_{o\&m}$), saved electricity (C_e), and saved heating energy (C_f). Operating and maintenance cost was taken as 10% of the investment cost (Arslan and Kilic, 2021), whereas the electricity tariff (C_e) was taken as 0.14 $/kWh (EPDK, 2022). The cost of the saved heating energy was included as 12.92 $/MWh in calculations (Iz-Geo, 2022). B_t is given as:

$$B_t = C_e + C_f - C_{o\&m} \tag{37}$$

The investment cost was determined by taking the current system into account. So, the investment costs of the TES system (C_{TES}), PCM (C_{PCM}), and additional panel radiator (C_{pr}) were handled in the analysis.

$$I = C_{TES} + C_{PCM} + C_{pr} \tag{38}$$

Here, C_{PCM} was taken as 95 $/ton (Indiamart, 2022) where C_{pr} was taken as 77.55 $/m (Demirdokum, 2022). C_{TES} was calculated according to the equation obtained from the manufacturer data (TUREVMAK, 2022):

$$C_{TES} = 7.489 \bullet 10^{-7}\left(n_{pipe}\right)^4 - 4.915 \bullet 10^{-4}\left(n_{pipe}\right)^3 + 0.106\left(n_{pipe}\right)^2 - 6.106 n_{pipe} + 741.040 \tag{39}$$

Table 6
The formed cases of TES-based S-GDHS.

Cases	T_1 (°C)	T_2 (°C)*	T_3 (°C)*	T_4 (°C)	T_5 (°C)*	T_6 (°C)	T_7 (°C)	T_8 (°C)	T_9 (°C)	PCM
Case 1	100	99.89	68.48	95.00	94.91	55	45	60	59.94	RT55
Case 2	100	99.89	68.49	95.00	94.91	55	40	60	59.94	RT55
Case 3	100	99.89	68.50	95.00	94.91	55	35	60	59.94	RT55
Case 4	100	99.89	68.51	95.00	94.91	55	30	60	59.94	RT55
Case 5	100	99.89	68.52	95.00	94.91	55	25	60	59.94	RT55
Case 6	95	94.89	63.48	90.00	89.91	50	40	55	54.95	RT50
Case 7	95	94.89	63.49	90.00	89.91	50	35	55	54.95	RT50
Case 8	95	94.89	63.50	90.00	89.91	50	30	55	54.95	RT50
Case 9	95	94.89	63.50	90.00	89.91	50	25	55	54.95	RT50
Case 10	95	94.89	63.48	90.00	89.92	50	40	58	57.95	RT50
Case 11	95	94.89	63.49	90.00	89.92	50	35	58	57.95	RT50
Case 12	95	94.89	63.50	90.00	89.92	50	30	58	57.95	RT50
Case 13	95	94.89	63.50	90.00	89.92	50	25	58	57.95	RT50
Case 14	90	89.90	58.58	85.00	84.93	45	35	53	52.96	RT47
Case 15	90	89.90	58.51	85.00	84.93	45	30	53	52.96	RT47
Case 16	85	84.90	53.67	80.00	79.93	42	32	42	47.96	RT42
Case 17	100	99.89	68.78	95.00	94.92	50	40	63	62.95	RT54HC
Case 18	100	99.89	68.78	95.00	94.92	50	35	63	62.95	RT54HC
Case 19	100	99.89	68.79	95.00	94.92	50	30	63	62.95	RT54HC
Case 20	100	99.89	68.79	95.00	94.92	50	25	63	62.95	RT54HC
Case 21	100	99.89	68.79	95.00	94.92	45	35	63	62.95	RT54HC
Case 22	100	99.89	68.79	95.00	94.92	45	30	63	62.95	RT54HC
Case 23	100	99.89	68.53	95.00	94.92	45	30	63	62.95	RT54HC
Case 24	100	99.89	68.52	95.00	94.92	45	30	63	62.95	RT50
Case 25	100	99.89	69.06	95.00	94.88	43	31	48	47.94	RT44HC
Case 26	100	99.89	69.06	95.00	94.88	43	31	50	49.94	RT44HC
Case 27	100	99.89	69.06	95.00	94.89	43	31	55	54.94	RT44HC
Case 28	100	99.89	69.06	95.00	94.89	43	31	60	54.94	RT44HC
Case 29	100	99.89	69.05	95.00	94.92	43	31	64	63.95	RT44HC
Case 30	95	94.89	64.03	90.00	89.92	43	31	58	57.95	RT44HC
Case 31	95	94.89	64.03	90.00	89.92	43	31	55	58.95	RT44HC
Case 32	95	94.89	64.03	90.00	89.90	43	31	50	49.95	RT44HC
Case 33	95	94.89	64.03	90.00	89.90	43	31	48	47.95	RT44HC
Case 34	90	89.90	59.00	85.00	84.91	43	31	48	47.95	RT44HC
Case 35	90	89.90	59.00	85.00	84.91	43	31	50	47.95	RT44HC
Case 36	90	89.90	59.01	85.00	84.93	43	31	54	53.96	RT44HC
Case 37	85	84.90	53.98	80.00	79.93	43	31	48	47.96	RT44HC

* calculated values.

2.8. Environmental evaluation

In the environmental evaluation, the probable generation of emissions was considered. In this regard, the emission prevented by saving electricity was considered to be sourced from lignite since the region's electricity is supplied by a coal-fired power plant. On the other hand, the emission prevented by saving heating energy was considered to be sourced from natural gas since it is the most used source in Turkey. The basis of the emissions is given in Table 5 (Arslan et al., 2022; Arslan and Erbas, 2021).

2.9. Multi-criteria decision analysis

Multi-criteria analysis of the energy systems is useful on decision making problems (Arslan et al., 2021; Arslan and Arslan, 2022). Efficiency Analysis Technique with Output Satisficing (EATWOS) is a new technique with satisfactory solutions based on output. It is a handy tool for determining the optimal solution of energy problems (Arslan et al., 2019a, 2019b). In view of input values, it is a technique that can give comparative results for selected outputs. EATWOS implementation steps are summarized below (Peters and Zelewski, 2006). Depending on the input (x) and output (y) values, the input ($\underline{X}$) and output ($\underline{Y}$) matrices are respectively formed as follows:

$$\underline{X} = \begin{bmatrix} x_{11} & \cdots & x_{1K} \\ \vdots & \ddots & \vdots \\ x_{I1} & \cdots & x_{IK} \end{bmatrix} \quad x_{ik} \in \mathbb{R}_{\geq 0} \quad \forall_i = 1, \ldots, \quad I \quad \forall_k = 1, \ldots, \quad K \tag{40}$$

$$\underline{Y} = \begin{bmatrix} y_{11} & \cdots & y_{1J} \\ \vdots & \ddots & \vdots \\ y_{I1} & \cdots & y_{IJ} \end{bmatrix} \quad y_{ij} \in \mathbb{R}_{\geq 0} \quad \forall_i = 1, \ldots, \quad I \quad \forall_j = 1, \ldots, \quad J \tag{41}$$

Then, these matrices are normalized using the following equations in terms of input and out values:

$$s_{ik} = \frac{x_{ik}}{\sqrt{\sum_{i=1}^{K} x_{ik}^2}} \tag{42}$$

$$r_{ij} = \frac{y_{ij}}{\sqrt{\sum_{i=1}^{I} y_{ik}^2}} \tag{43}$$

In the third step, the distance matrices are calculated for the input (ip_{ik}) and output (op_{ik}) values. In this context, the following distance measurement expressions are used for the input and output values, respectively.

$$ip_{ik} = 1 + s_{ik} - s_k^* \tag{44}$$

$$op_{ik} = 1 + r_{ij} - r_j^* \tag{45}$$

where s_k^* and r_j^* are normalized maximum input and output values, respectively. These values are given as follows:

$$s_k^* = \min_i \{s_k\} \tag{46}$$

$$r_j^* = \max_i \{r_j\} \tag{47}$$

Finally, the efficiency values are calculated as follows:

$$E_i = \frac{\sum_{j=1}^{J} v_j \bullet op_{ij}}{\sum_{k=1}^{K} w_k \bullet ip_{ik}} \tag{48}$$

where w_k and v_j are the input and output parameters weights, respectively.

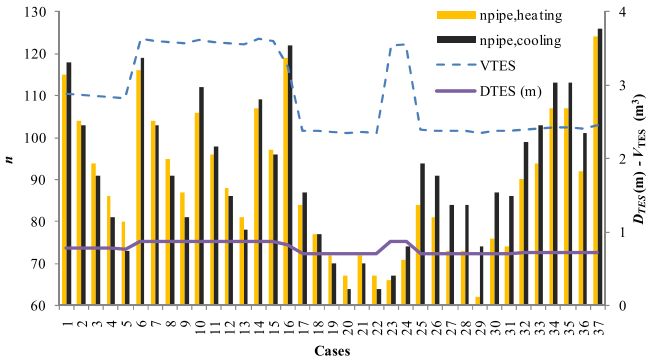

Fig. 6. TES system characteristics.

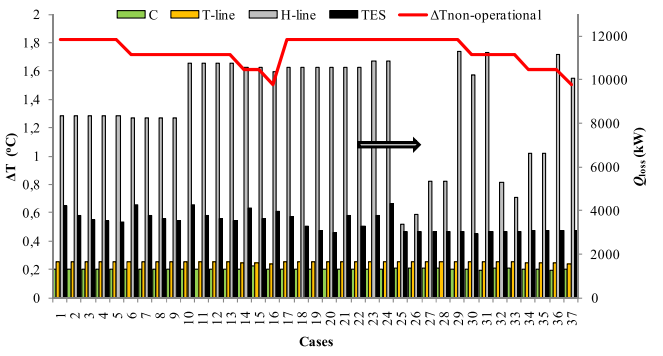

Fig. 7. Heat losses occurred in the subsystems.

3. Results and discussion

The S-GDHS currently operates using a substation heat exchanger to feed the heating circuits (panel radiators). In this study, a TES-based GDHS is proposed to change the heat exchangers by a TES system. So, the TES-based S-DGHS was designed to prevent the extravagant use of geothermal sources. The considered 37 cases are given in Table 6.

According to Table 6, the TES system was designed in the form of a shell and tube type. Two kinds of tubes, namely heating and cooling pipes, were included in the shell. Heating pipes store the daily required energy based on peak demand. Cooling pipes transfer this energy to the heating circuit system. The shell side is a closed system working as a thermo-siphon. The required pipe numbers for heating and cooling, the TES system (D_{TES}) diameter, and TES system volume (V_{TES}) are shown in Fig. 6.

According to Fig. 6, the number of heating pipes ($n_{pipe,heating}$) varies between 62 and 124, whereas the number of cooling pipes ($n_{pipe,cooling}$) vary between 64 and 126. The TES system volume (V_{TES}) varies between 2.35 and 3.63 m^3, whereas the diameter of the TES system (D_{TES}) varies between 0.707 and 0.877 m. The heat transfer coefficient, which changes by temperature, is the most decisive factor on the number of pipes. Along with the number of pipes, the kind of PCM (latent heat capacity) is the main factor on the volume of TES. Heat losses were also considered in the designed system and given in Fig. 7.

According to Fig. 7, the heat losses in the TES system vary between 2936 kW and 4295 kW. These losses were added to the H-line system by increasing the related mass flow rate. These ranges are between 1584 kW and 1665 kW, 1286 kW and 1441 kW, 3384 kW and 11,324 kW for T-line, C, and H-line, respectively. Also, the non-operational conditions, in which the system is not feeding the HC, were considered. The maximum temperature decrease was recorded as 1.82 °C for a whole day of non-operational conditions. So, this temperature fluctuation would not affect the cut-in and cut-off processes system operation. One of the most important parameters is the power

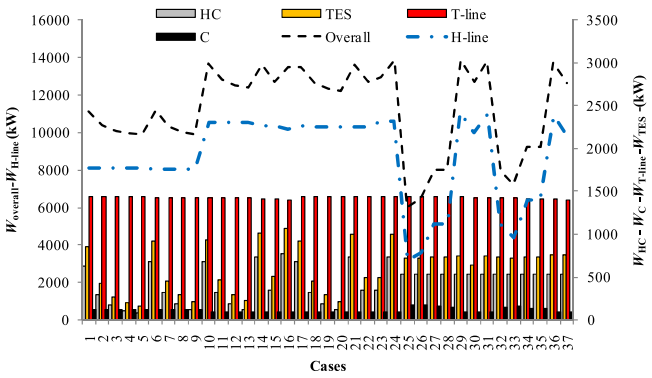

Fig. 8. The required pump powers.

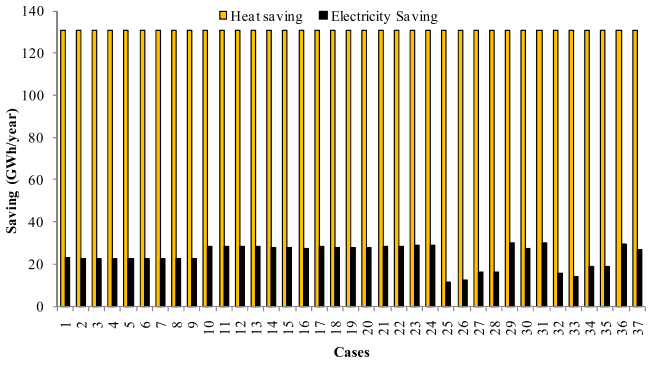

Fig. 9. Saving values of TES-based SGDHS.

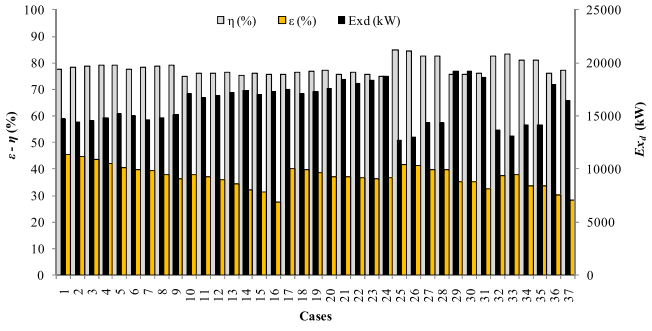

Fig. 10. Results of energy and exergy analyses.

consumption by pumps to save energy through the TES system integration. All the required pump powers were calculated, and the results are given in Fig. 8.

According to Fig. 8, the most required pump power was recorded in the H-line with 11,067 kW. In the H-line, the minimum power was recorded as 3154 kW. So, these recorded amounts are significant considering the goal of this study. Under non-operational conditions, saving would be more important than heat loss under this circumstance. The required pump power varies between 155 kW and 1062 kW for the TES system. These ranges were recorded as 1.396 kW and 1441 kW, 88.76 kW and 180.15 kW, 81.78 kW and 775.18 kW for T-line, C, and HC, respectively. The overall pump powers were calculated between 6032 kW and 13,889 kW. According to these calculations, the electricity saving was between 11.34 and 30.24 GWh per year. The heat-saving was calculated as a constant value of 130.94 GWh per year. The variation of the energy saving is shown in Fig. 9.

According to Fig. 9, although the system savings are sourced from heat and electricity, the variation of the savings is sourced from

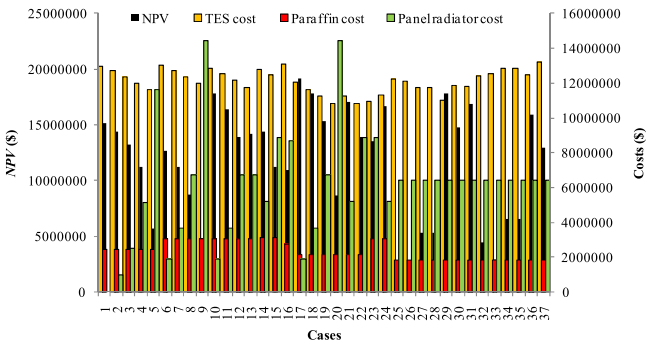

Fig. 11. Results of NPV analysis.

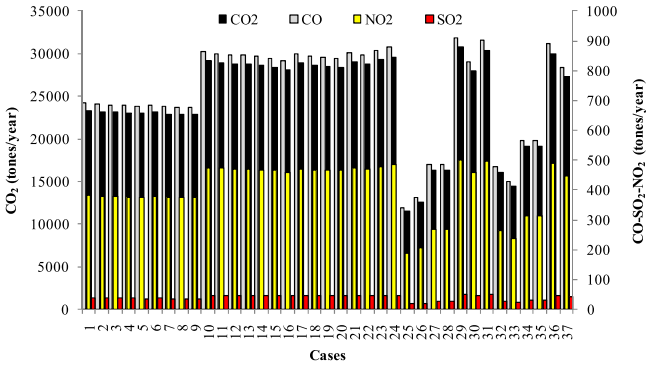

Fig. 12. Results of environmental evaluation sourced by electricity saving.

electricity. The heat demands are constant on a yearly basis (also daily basis) since it is required energy for the residences that should be supplied for heating purpose. However, the electricity saving is variable since it is sourced by the equipment running on a design basis. The formed cases were analyzed by energy and exergy tools. The variation in energy efficiency, exergy efficiency, and exergy destruction rates are given in Fig. 10.

According to Fig. 10, the exergy destruction rate of the overall system varies between 12,676 kW and 19,242 kW. The most exergy destructive design was determined as Case 29. The energy efficiency of the overall system varies between 74.86% and 84.89%. The most energy-efficient design was determined as Case 25. The exergy efficiency of the overall system varies between 27.62% and 45.33%. The most exergy efficient design was determined as Case 1. The designed system was evaluated from the economic point of view by the NPV method. The results are shown in Fig. 11.

According to Fig. 11, TES cost vary between 10,851,978 $ and 13,215,639 $ where the PCMs vary between 1,861,475 $ and 3,150,188 $. The cost of an additional panel radiator equals 14,454,425 $. So, the NPV values vary between 845,092 and 19,149,642 $. The most investable case was determined as Case 17. The environmental evaluation was conducted based on saved electricity and fuel. The obtained results sourced by electricity savings are shown in Fig. 12.

According to Fig. 12, the prevented CO_2 emission varies between 11,530 tons and 30,745 tons per year. The values for other constituents vary between 341.75 and 911.29 tons, 188.55 and 502.78 tons, 18.51 and 49.35 tons for CO, NO_2, and SO_2, respectively. For the annually saved fuel, these emissions were determined as 1,208,016 tons, 145.69 tons, and 20,961 tons for CO_2, CO, and NO_2, respectively. There is no SO_2 emission since the supplied natural gas does not include sulfur. According to these records, the most environment-friendly design was determined as Case 29. Finally, a multi-criteria decision-making analysis (EATWOS) was conducted to determine the most effective design. The input values were T_1, T_6, T_7, T_8, *and* $T_{melting}$ since they play a vital role in

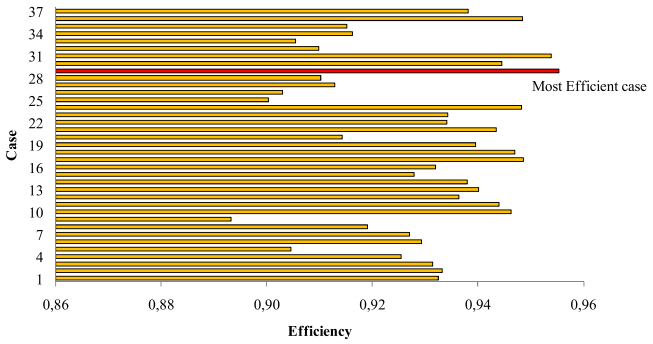

Fig. 13. EATWOS results and optimal solution.

the designs. From an environmental, engineering, and investor perspective, the output values were selected as CO_2 emission saving, exergy efficiency (ε), and NPV. Since all the input and output parameters have equal importance degrees, the related weights are equal. Therefore, it was included in the analysis as 1/5 and 1/3 for the input and output parameters, respectively. The results of EATWOS are given in Fig. 13.

According to Fig. 13, the efficiency values change between 0.8932 and 0.9553. Case 29 is the most environmentally friendly case with the highest emission reduction. The exergy efficiency was calculated as 35.11% for the minimum inlet conditions (T_1=100 °C, T_6=43 °C, T_7=31 °C and T_8=64 °C). The available PCM has a melting temperature of 43 °C in this case. This case has a NPV value of 17,860,504 $. This value shows that the proposed system is investable at a considerable rate. The analysis also showed that low-temperature circuits (43/31 °C) are more effective for heating systems in residences. By this TES-based GDHS, the increase in exergy efficiency of the system was determined as 15.27% compared to the old (current) one with an exergy efficiency of 30.46%. According to the three key parameters of efficiency analysis, it was concluded that NPV and environmental aspects are more powerful parameters on the multi-criteria decision-making process in comparison to exergy outputs. When the efficiency analysis with single output was conducted, the most efficient cases were determined as Case 25 for the exergy efficiency, Case 31 for CO_2 reduction and Case 29 for NPV. From this point of view, NPV is the most powerful parameter. The most efficient design was determined as Case 29 according to the simultaneous evaluation of all output parameters of exergy efficiency, net present value and CO_2 emission. This case is the most environmentally friendly design with the highest emission reduction. Although the exergy efficiency is relatively low compared to others, the higher NPV and emission reduction values make this case the most efficient one. In this case, the inlet temperature of the geothermal fluid of heat GDHS (T_1) is 100 °C, whereas the outlet temperature (T_3) is 69.05 °C. The heating circuit temperature is 43/31 °C at the inlet and outlet of the panel radiators, respectively. The outlet temperature of the H-line at the TES substation (T_8) is 64 °C for the PCM with a melting point of 43 °C. The thermophysical characteristics of Case 29 are given in Table 7. The energy and exergy analysis results obtained according to these characteristics are given in Table 8.

According to Table 8, the highest exergy destruction occurs in the H-line depending on the higher pump power requirement and heat losses. In this regard, the exergy efficiency of the H-line was determined as 67.73%. The lowest exergy efficiency was observed for the TES system at 49.24%, depending on the higher heat losses. The exergetic efficiency of the overall system was determined as 35.11%. The NPV results of Case 29 are given in Table 9.

According to Table 9, a NPV is obtained equal to 17,860,504 $. The system's payback period was determined as 3 years with a total investment cost of 19,353,111 $.

4. Conclusions

A new design was made for the Simav Geothermal District Heating System (S-GDHS) in Turkey. Since the current system uses a heat exchanger located in the substations in continuous operation with enormous waste heat and daily electricity consumption, a Thermal Energy Storage (TES) based substation was integrated into the Geothermal District Heating System (GDHS) to save electricity, and reduce heat loss and emissions. A shell and tube type latent heat TES system was designed and coupled with the heating circuit (HC) for controlling the system operation. The formed S-GDHS was analyzed parametrically in terms of temperature and Phase Change Material (PCM) by energy and exergy methods. The obtained cases were evaluated from an economic aspect by the Net Present Value (NPV) method. Finally, the designs were evaluated from the environmental aspect. The obtained results were then analyzed by the efficiency analysis technique with output satisficing (EATWOS). It is available to prevent CO2 emissions of over one

Table 7
Thermophysical characteristics of optimal TES-based S-GDHS.

Points	Fluids	$\dot{m}$ (kg/s)	T (°C)	h (kJ/kg)	s (kJ/kgK)	v (m^3/kg)	ψ (kJ/kg)	$\dot{E}$ (kW)	$\dot{E}x$ (kW)
0	H_2O	–	25.00	104.82	0.3674	–	–	–	–
1	Geofluid	462.00	100.00	419.17	1.3072	0.001043	34.12	193655.51	15764.57
2	Geofluid	462.00	99.89	418.68	1.3059	0.001043	34.02	193432.34	15719.47
3	Geofluid	462.00	69.05	289.10	0.9436	0.001022	12.47	133563.01	5760.38
4	H_2O	450.00	95.00	398.09	1.2504	0.001040	29.98	179141.30	13489.07
5	H_2O	450.00	94.92	397.74	1.2495	0.001039	29.91	178985.66	13459.33
6	H_2O	1118.80	43.00	180.08	0.6122	0.001009	2.28	201478.11	2546.87
7	H_2O	1118.80	31.00	129.91	0.4505	0.001005	0.30	145348.11	340.47
8	H_2O	450.00	64.00	263.75	0.8688	0.001019	9.41	116023.93	4139.35
9	H_2O	450.00	63.95	263.52	0.8682	0.001019	9.38	115923.95	4128.09

Table 8
Energy and exergy analysis results of optimal TES-based S-GDHS.

Components	$\dot{W}$ (kW)	$\dot{Q}$ (kW)	$\dot{E}_i$ (kW)	$\dot{E}_o$ (kW)	$\dot{E}x_i$ (kW)	$\dot{E}x_o$ (kW)	$\dot{E}x_d$ (kW)	η (%)	ε (%)
T- line	1441.36	-1664.53	193655.51	193432.34	15764.57	15719.47	1152.11	99.15	93.30
C	93.52	-1290.92	313901.71	312704.31	20156.91	19249.45	793.89	99.59	96.08
H- line	11066.77	-11324.13	299712.39	299455.02	17938.24	17896.77	9359.08	96.36	67.73
TES	749.38	-3033.96	324333.77	322049.19	13799.80	6996.03	7384.94	99.07	49.24
HHC	538.31	-56668.31	201478.11	145348.11	2546.87	340.47	552.16	99.05	82.10
Overall system	***13889.35***	***-17313.53***	***193655.51***	***133563.01***	***15764.57***	***5760.38***	***19242.18***	***75.87***	***35.11***

Table 9
NPV analysis results of optimal TES-based S-GDHS.

	Years					
	Present	1	5	10	15	20
Investment						
TES cost	-11,034,754.85					
Panel radiator addition cost	-6456,881.47					
Paraffin	-1861,474.91					
Total	-19,353,111.23					
Cash flow						
Expenses						
Operating & Maintenance		55,173.77	55,173.77	55,173.77	55,173.77	55,173.77
Electricity benefit		4235,220.58	4235,220.58	4235,220.58	4235,220.58	4235,220.58
Heat benefit		1691,290.86	1691,290.86	1691,290.86	1691,290.86	1691,290.86
Salvage	1935,311.12					
Total cash flow	-17,417,800.11	5871,337.66	5871,337.66	5871,337.66	5871,337.66	5871,337.66
Cumulative cash flow	-17,417,800.11	-11,546,462.45	11,938,888.20	41,295,576.52	70,652,264.83	100,008,953.14
Discount rate (15.75%)	1.000	0864	0.481	0.232	0.111	0.054
Present value	-17,417,800.11	5072,429.95	2825,739.09	1359,962.90	654,518.70	315,004.72
NPV	**17,860,504.28**					

million tons per annum. The new system is investable and profitable with considerable NPV values. The EATWOS is a powerful tool to decide the optimal solution for energy systems including multiple design criteria. However, the weights of the EATWOS analysis should be determined carefully since it directly would affect the results. In this regard, the determination of the priority of the requirements (outputs) and the learned opinions of the experts are critical issues.

Declaration of Competing Interest

The authors declare that they have no known competing financial interests or personal relationships that could have appeared to influence the work reported in this paper.

References

Akbulut, A., Oguz Arslan, O., Arat, H., Erbas, O., 2021. Important aspects for the planning of biogas energy plants: malatya case study. Case Stud. Therm. Eng. 26, 101076.

Arat, H., Arslan, O., 2017a. Exergoeconomic analysis of district heating system boosted by the geothermal heat pump. Energy 119, 1159–1170.

Arat, H., Arslan, O., 2017b. Optimization of district heating system aided by geothermal heat pump: a novel multistage with multilevel ANN modelling. Appl. Therm. Eng. 111, 608–623.

Arslan, A.E., Acar, M.S., Arslan, O., 2019a. Optimization of O-type ORC-Binary geothermal power plant: EATWOS analysis. BSEU J. Sci. 6, 222–236. https://doi.org/10.35193/bseufbd.601745.

Arslan, A.E., Arslan, O., Kandemir, S.Y., 2021. AHP–TOPSIS hybrid decision-making analysis: simav integrated system case study. J. Therm. Anal. Calorim. 145, 1191–1202.

Arslan, O., Arslan, A.E., 2022. Pareto principle-based advanced exergetic evaluation of geothermal district heating system: simav case study. J. Build. Eng. 58, 105035.

Arslan, O., Erbas, O., 2021. Investigation on the improvement of the combustion process through hybrid dewatering and air pre-heating process: a case study for a 150 MW coal-fired boiler. J. Taiwan Inst. Chem. Eng. 121, 229–240.

Arslan, O., Kilic, D., 2021. Concurrent optimization and 4E analysis of organic Rankine cycle power plant driven by parabolic trough collector for low-solar radiation zone. Sustain. Energy Technol. Assess. 46, 101230.

Arslan, O., Kose, R., 2010. Exergoeconomic optimization of integrated geothermal system in Simav, Kutahya. Energy Convers. Manag. 51, 663–676.

Arslan, O., Ozgur, M.A., Kose, R., Tugcu, A., 2009a. Exergoeconomic evaluation on the optimum heating circuit system of Simav geothermal district heating system. Energy Build. 41, 1325–1333.

Arslan, O., Ozgur, M.A., Yildizay, H.D., R. Kose, R., 2009b. Fuel effects on optimum insulation thickness: an exergetic approach. Energy Sources Part A Recovery Util. Environ. Eff. 32, 128–147.

Arslan, O., Arslan, A.E., Acar, M.S., 2019b. Multi-criteria making-decision modeling of b-type ORC-binary geothermal power plant: EATWOS Analysis. BSEU J. Sci. 6, 29–48. https://doi.org/10.35193/bseufbd.561668.

Arslan, O., Acikkalp, E., Genc, G., 2022. A multi-generation system for hydrogen production through the high-temperature solid oxide electrolyzer integrated to 150 MW coal-fired steam boiler. Fuel 315, 123201.

Bertrand, O., Binet, B., Combeau, H., Couturier, S., Delannoy, Y., Gobin, D., Lacroix, M., Le Quere, P., Medale, M., Mencinger, J., Sadat, H., Vieir, G., 1999. Melting driven by natural convection A comparison exercise: first results. Int. J. Therm. Sci. 38, 5–26.

Cabeza, L.F., Palomba, V., 2022. The role of thermal energy storage in the energy system. In: Cabeza, Luisa F. (Ed.), Encyclopedia of Energy Storage. Elsevier, pp. 338–350.

CBRT (Central Bank of Republic of Turkey). 2022. Inflation report, Available from: ⟨https://www.tcmb.gov.tr/wps/wcm/connect/EN/TCMB+EN/Main+Menu/Core+Functions/Monetary+Policy/Rediscount+and+Advance+Interest+Rates⟩. Last Access: April 7th, 2022.

Cengel, Y.A., Boles, J.M., 2018. Fluid mechanics: Fundamentals and Applications, 4th edition.,. McGraw Hill,, New York.

Cunha, J.M., Faria, A.S., Soares, T., Mourão, Z., Nereu, J., 2022. Decarbonization potential of integrating industrial excess heat in a district heating network: the Portuguese case. Clean. Energy Syst. 1, 100005.

Dahash, A., Ochs, F., Tosatto, A., 2021. Techno-economic and exergy analysis of tank and pit thermal energy storage for renewables district heating systems. Renew. Energy 180, 1358–1379.

Demirdokum. 2022. PKKP 600 type panel radiator. Available from: ⟨https://www.cimri.com/radyator/en-ucuz-demirdokum-pkkp-600–1000-panel-plus-radyator-fiyatlari,503553⟩. Last Access: April 7th, 2022.

Dorotić, H., Pukšec, T., Duić, N., 2019. Economical, environmental and exergetic multi-objective optimization of district heating systems on hourly level for a whole year. Appl. Energy 251, 113394.

EPDK (Energy Market Regulatory Authority of Rebuplic of Turkey). 2022. Electricity tariffs. Available from: ⟨https://www.epdk.gov.tr/Detay/Icerik/3–1327/elektrik-faturalarina-esas-tarife-tablolari⟩. Last Access: April 7th, 2022.

Genceli, O.F., 1999. Heat Exchangers. Birsen Publication, Istanbul (in Turkish).

Halaj, E., Pająk, L., Papiernik, B., 2022. Simulation study of the Lower Cretaceous geothermal reservoir for aquifer thermal energy storage. Environ. Geochem. Health 2022 (44), 2253–2279.

He, Z., Farooq, A.S., Guo, W., Zhang, P., 2022. Optimization of the solar space heating system with thermal energy storage using data-driven approach. Renew. Energy 190, 764–776.

Hemmatabady, H., Welsch, B., Formhals, J., Sass, I., 2022. AI-based enviro-economic optimization of solar-coupled and standalone geothermal systems for heating and cooling. Appl. Energy 311, 118652.

Huang, Y., Pang, Z., Kong, Y., Watanabe, N., 2021. Assessment of the high-temperature aquifer thermal energy storage (HT-ATES) potential in naturally fractured geothermal reservoirs with a stochastic discrete fracture network model. J. Hydrol. 603, 127188.

Indiamart. 2022. The price of paraffin wax. Available from: ⟨https://www.indiamart.com/proddetail/chlorinated-paraffin-wax-22420468491.html⟩. Last Access: April 7th, 2022.

Iz-Geo (Izmir Geothermal A.Ş). 2022. Heating tariffs. Available from: ⟨https://www.izmirjeotermal.com.tr/islemler-ucret-tarifeleri-2021–2022-isitma-sezonu⟩. Last Access: April 7th, 2022.

Jiangyin M.&C.Heat Parts, 2022a. NT250L type heat exchangers. Available from: ⟨https://turkish.heat-exchangergasket.com/sale-14362173-titanium-0–5mm-nt250l-plate-heat-exchanger-plate-for-sea-water-fluid.html⟩. Last access: April 7th, 2022.

Jiangyin M.&C.Heat Parts, 2022b. Tranter GC26 type heat exchangers. Available from: ⟨https://turkish.heat-exchangergasket.com/sale-14301136-tranter-gc26-small-pressure-plate-heat-exchanger-plates-and-gaskets.html⟩. Last access: April 7th, 2022.

Kim, D., Lee, D., Heo, J., Kim, M., 2018. Empirical results and operational cost analysis of geothermal heat pump system using thermal energy storage in cooling season. Korean J. Air-Cond. Refrig. Eng. 30, 167–174.

Knudsen, B.R., Rohde, D., Kauko, H., 2021. Thermal energy storage sizing for industrial waste-heat utilization in district heating: a model predictive control approach. Energy 234, 121200.

Kyriakis, S.A., Younger, P.L., 2016. Towards the increased utilization of geothermal energy in a district heating network through the use of a heat storage. Appl. Therm. Eng. 94, 99–110.

Li, H., Hou, J., Hong, T., Ding, Y., Nord, N., 2021. Energy, economic, and environmental analysis of integration of thermal energy storage into district heating systems using waste heat from data centers. Energy 219, 119582.
Mäki, E., Kannari, L., Hannula, I., Shemeikka, J., 2021. Decarbonization of a district heating system with a combination of solar heat and bioenergy: a techno-economic case study in the Northern European context. Renew. Energy 175, 1174–1199.
Matuszewska, D., Kuta, M., Olczak, P., 2020. Techno-economic assessment of mobilized thermal energy storage system using geothermal source in Polish conditions. Energies 13, 3404.
Mohaghegh, M.R., Tasnim, S.H., Mahmud, S., 2022. A geometrical optimization and comparison study on the charging and discharging performance of shell-and-tube thermal energy storage systems. J. Energy Storage 51, 104549.
MSTS (Meteorological Service of Turkish State). Data of daily average outdoor air temperature of 2015–2019, July 2022a.
MSTS (Meteorological Service of Turkish State). Data of daily average soil temperature of 2015–2019, July 2022b.
Peters M.L., Zelewski S. Efficiency Analysis Under Consideration of Satisficing Levels for Output Quantities. In Proceedings of the 17th Annual Conference of the Production and Operations Management Society (POMS), April 28-May 01, 2006, Boston, USA.
Rezaie, B., Reddy, B.V., Rosen, M.A., 2015. Exergy analysis of thermal energy storage in a district energy application. Renew. Energy 74, 848–854.
RUBITHERM, 2022. Phase change materials. Available from: ⟨https://www.rubitherm.eu/en/index.php/productcategory/organische-pcm-rt⟩. Last access: April 7th, 2022.
Saloux, E., Candanedo, J.A., 2021. Model-based predictive control to minimize primary energy use in a solar district heating system with seasonal thermal energy storage. Appl. Energy 291, 116840.
Siddiqui, S., Macadam, J., Barrett, M., 2021. The operation of district heating with heat pumps and thermal energy storage in a zero-emission scenario. Energy Rep. 7, 176–183.
Tenpierik, M., Wattez, Y., Turrin, M., Cosmatu, T., Tsafou, S., 2019. Temperature control in (Translucent) phase change materials applied in facades: a numerical study. Energies 12, 3286.
TSE (Turkish Standards Institution). TS 825: Thermal insulation requirements for buildings; May 2008.
TUREVMAK, 2022. Quotation for TES System Production. Turevmak Machinery, Natural gas, Heating Systme LLC, Bozuyuk, Turkey.
Ucar, M., Arslan, O., 2021. Assessment of improvement potential of a condensed combi boiler via advanced exergy analysis. Therm. Sci. Eng. Prog. 23, 100853, 2021.
Wu, Y., Li, D., Jiang, W., Zhu, S., Zhao, X., Arici, M., Tuncbilek, E., 2022. Energy storage and exergy efficiency of a shell and tube latent thermal energy storage unit with non-uniform length and distributed fins. Sustain. Energy Technol. Assess. 53, 102362.
Yuncu, H., Kakac, S., 1999. Basic Heat Transfer. Bilim Publishing, Ankara (in Turkish).